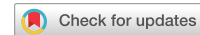


communications

earth & environment

ARTICLE



<https://doi.org/10.1038/s43247-022-00369-x>

OPEN

Deep water inflow slowed offshore expansion of the West Antarctic Ice Sheet at the Eocene-Oligocene transition

Gabriele Uenzelmann-Neben ^{1✉}, Karsten Gohl ¹, Katharina Hochmuth ^{1,2}, Ulrich Salzmann ³, Robert D. Larter ⁴, Claus-Dieter Hillenbrand ⁴, Johann P. Klages ¹ & Science Team of Expedition PS104*

The stability of the West Antarctic Ice Sheet is threatened by the incursion of warm Circumpolar Deepwater which flows southwards via cross-shelf troughs towards the coast there melting ice shelves. However, the onset of this oceanic forcing on the development and evolution of the West Antarctic Ice Sheet remains poorly understood. Here, we use single- and multichannel seismic reflection profiles to investigate the architecture of a sediment body on the shelf of the Amundsen Sea Embayment. We estimate the formation age of this sediment body to be around the Eocene-Oligocene Transition and find that it possesses the geometry and depositional pattern of a plastered sediment drift. We suggest this indicates a southward inflow of deep water which probably supplied heat and, thus, prevented West Antarctic Ice Sheet advance beyond the coast at this time. We conclude that the West Antarctic Ice Sheet has likely experienced a strong oceanic influence on its dynamics since its initial formation.

¹ Alfred-Wegener-Institut Helmholtz-Zentrum für Polar- und Meeresforschung, Bremerhaven, Germany. ² School of Geography, Geology and the Environment, University of Leicester, Leicester, UK. ³ Department of Geography and Environmental Sciences, Northumbria University, Newcastle upon Tyne, UK. ⁴ British Antarctic Survey, Cambridge, UK. *A list of authors and their affiliations appears at the end of the paper. ✉email: gabriele.uenzelmann-neben@awi.de

Today, 25–35% of the West Antarctic Ice Sheet (WAIS) drain into the Amundsen Sea Embayment (ASE)^{1,2}. Warm Circumpolar Deepwater (CDW) is currently upwelling on the ASE slope and then flows along the eastern and central parts of deep bathymetric troughs at 118° W (Dotson-Getz Trough DGT), 113°W (Pine Island Trough West PITW), and 108–102°W (Pine Island Trough East PITE and Abbot Trough AT) across the up to 400 km wide continental shelf to the coast^{3,4} (Fig. 1). CDW then impinges into sub-ice shelf cavities and reaches the WAIS grounding zones, thereby causing sub-ice shelf melting and threatening the stability of the WAIS (e.g., refs. 5–8). Study of proxies in shelf sediment cores indicates similar sensitivity extends over millennia⁹. Although modelling studies simulate past WAIS collapses driven primarily by warm water incursion, e.g., during the Pliocene and some Quaternary interglacial periods^{10,11}, there is little observational evidence recording the

effects of oceanographic circulation on the longer term history of the ice sheet. This applies also to its initial advance onto the continental shelf.

Continental-scale Antarctic ice sheets are reported to have reached sea level during the EOT following a drop in temperature and atmospheric CO₂, which is documented in the Earliest Oligocene Oxygen Isotope Step (EOIS)^{12–16}. The influence of the ocean on the formation and advance/retreat of the Antarctic ice sheets at this time is unconstrained, since the ocean circulation and location of the Southern Ocean frontal system during the Oligocene are still debated^{17,18}. Various scenarios have been suggested based on regional studies. An East Antarctic Ice Sheet (EAIS) with a size fluctuating between larger and smaller than today was reconstructed for the time interval from 34.1 to 32.7 Ma based on clast abundance variability in shelf sediments from Cape Roberts in the southwestern Ross Sea¹⁶, whereas a

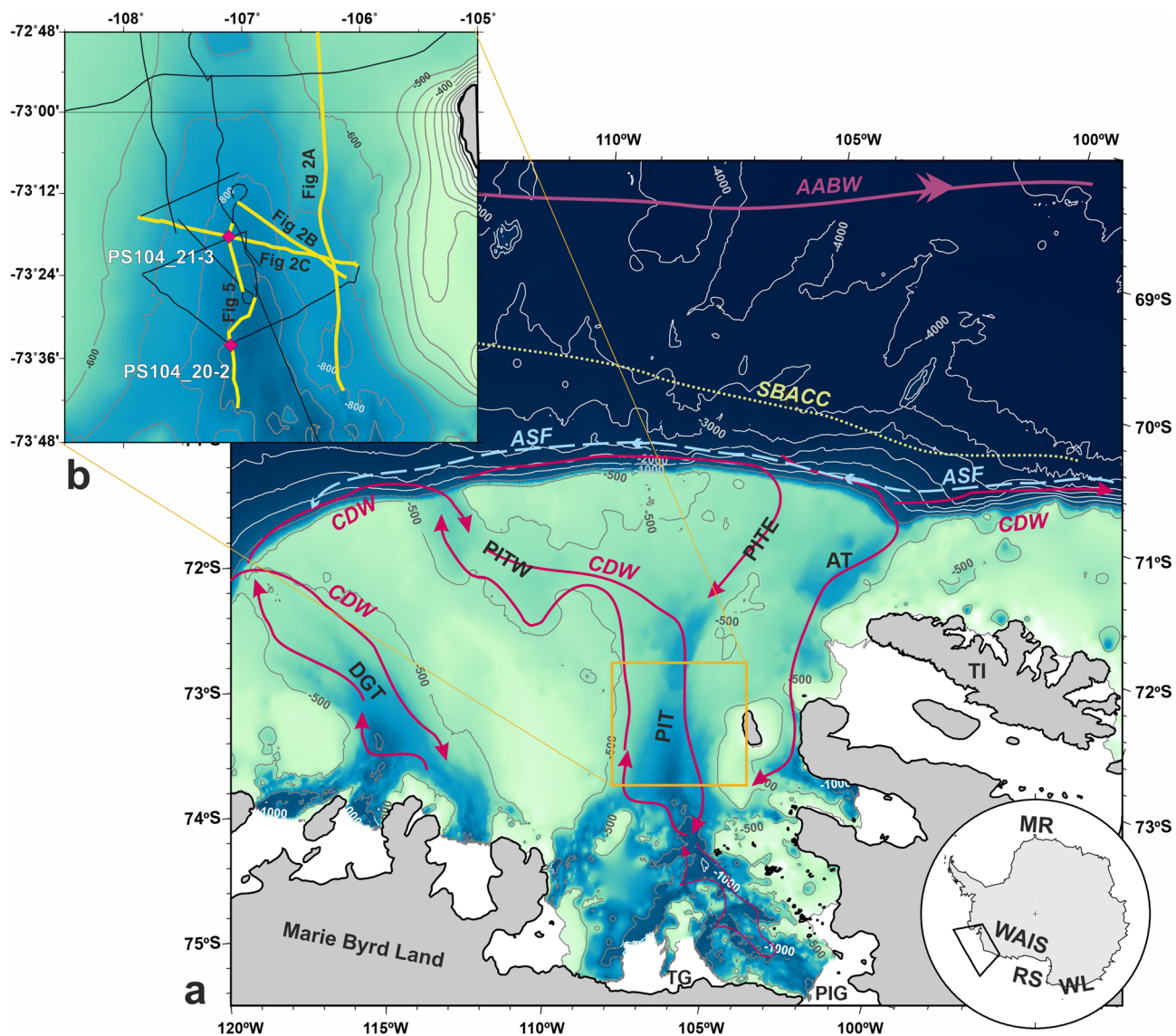


Fig. 1 Bathymetric map of the Amundsen Sea Embayment⁷⁸. **a** The present day active currents and water masses are shown schematically: AABW = Antarctic Bottomwater (purple double arrow)⁷⁹, SBACC = Southern Boundary of the Antarctic Circumpolar Current (yellow dotted)⁶⁰, ASF = Antarctic Slope Front (dashed light blue arrow) and CDW = Circumpolar Deepwater (red arrow)^{3,4,80,81}. The orange box shows the area enlarged in **(b)**. There, the locations of seabed drill Sites PS104_20-2 and PS104_21-3 (magenta diamonds) and seismic profiles (black lines, yellow lines displayed in Figs. 2 and 5) are shown. AT = Abbot Trough, DGT = Dotson-Getz Trough, MR = Maud Rise, PIG = Pine Island Glacier, PIT = Pine Island Trough, PITE = Pine Island Trough East, PITW = Pine Island Trough West, RS = Ross Sea, TG = Thwaites Glacier, TI = Thurston Island, WAIS = West Antarctic Ice Sheet, WL = Wilkes Land.

much reduced EAIS during the Early Oligocene, except for the time period from 33.6–32.1 Ma, was inferred from microfossils in sediments recovered offshore from the Wilkes Land region, East Antarctica¹⁹. Olivetti, et al.²⁰ concluded from the provenance of some of the clasts in the Cape Roberts sediments their origins from sources in the Transantarctic Mountains south of Byrd Glacier, implying that the WAIS may have advanced onto the Ross Sea shelf already during cold periods of the Early Oligocene from about 32 Ma onwards. Furthermore, both bathymetry and width of the Antarctic continental shelves and therefore the potential pathways of deep water flow towards the grounding zone of the ice sheet changed significantly since the onset of glaciation but the exact timing and rates of these changes remain uncertain^{21,22}. Knowledge of the palaeobathymetry is essential to identify possible water mass pathways such as troughs and channels, allowing the protrusion of warm deep water from the shelf break across the shelf and to the ice-sheet margins. Areas currently most vulnerable to deep water intrusions, such as the entire East Pacific margin of Antarctica, are severely under-represented in numerical simulations of palaeoenvironmental changes in Antarctica and the Southern Ocean across the EOT (including data-model comparisons). Reconstructions currently are only available for the East Tasman Plateau, New Zealand, and the Ross Sea²³.

Here, we present seismic reflection data combined with age information from shallow seabed drill cores from the ASE shelf to investigate potential palaeo-intrusions of deep water at the EOT by analysing the architecture of a sediment body identified in seismic profiles.

Results

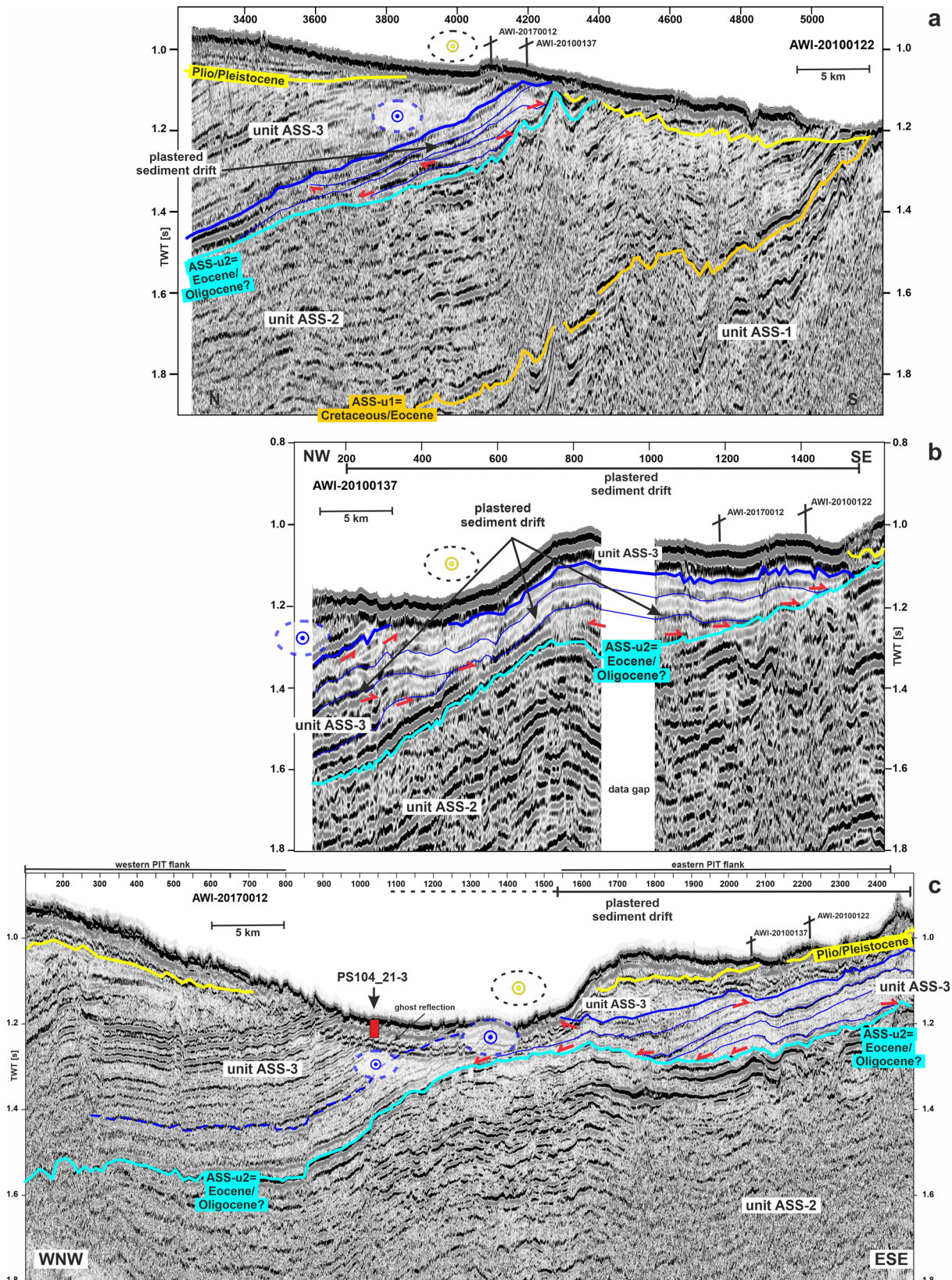
Seismic reflection data collected in Pine Island Trough (PIT) reveal an asymmetric sediment body at the eastern flank of the trough. The sediment body shows a well-stratified convex-up mounded morphology with its thicker part plastered against reflection ASS-u2, and it progressively thins towards the west (Fig. 2, blue horizon- top, cyan horizon- base of the sediment body). Reflection ASS-u2 generally slopes north-westward but shows a local high below the eastern part of today's PIT (Fig. 2). The sediment body is characterised by internal reflections (thin blue lines in Fig. 2) of good lateral continuity, which terminate (red arrows in Fig. 2) against the body's base reflection ASS-u2 (downlap, onlap) and top (truncation). The internal reflections mark subunits of the sediment body, which mimic its general shape and in their extent document the growth of the sediment body from the east towards the west (Fig. 2). The sediment body shows a maximum thickness of around 250 ms two-way travel time (~310 m using a mean conversion velocity of 2500 m/s as derived during processing) and covers an area of ~310 km². Its shallowest point lies in the southeast (Fig. 3), where the maximum in thickness is observed. The sediment body is well stratified, which is inconsistent with a glacial origin, e.g., formation as a grounding zone wedge or moraine, since those features typically possess a semi-transparent to chaotic seismic character^{24,25}. Based on its geometry and depositional pattern (convex-up morphology, mounded, well-stratified, good lateral continuity, progressive thinning), the sediment body is interpreted as a plastered sediment drift (see, e.g., Fig. 14.9 of Faugères and Stow²⁶). Sediment drifts are shaped by bottom currents interacting with bathymetry and available detritus^{27,28}. Plastered drifts are mounded sediment bodies located along gentle slopes swept by low-velocity bottom currents²⁹. The sediment body identified in PIT is not associated with a moat but plastered drifts do not necessarily have a moat^{30–32}.

The Coriolis effect strongly influences the internal flow structure of an oceanic current, deflecting the downstream velocity core towards the left on the southern hemisphere^{33,34}. Therefore, detritus supplied in meltwater plumes originating from the ice sheet margin in the south and flowing northwards would result in deposition on the western flank of a trough or channel, there shaping sediment drifts. The same would apply to northward transport of fluvial sediment input. However, reflection ASS-u2, which forms the sediment drift's base, does not show a trough. A sediment drift below the western flank of present-day PIT can neither be identified (Fig. 2c). A sediment body plastered to the eastward rising reflection ASS-u2 thus can only have been shaped by a southward flowing water mass (Fig. 4).

The plastered drift is identified in the lower part of seismic unit ASS-3 (Fig. 2, refs. ^{35,36}). Seismic unit ASS-3 forms one of six seismic units identified on the Amundsen Sea shelf (ASS)^{35,37}. The seismic units are separated by seismic unconformities ASS-u1 to ASS-u5. Seismic units ASS-1 and ASS-2 were sampled at seabed drill Site PS104_20-2 and found to be of Late Cretaceous age and Late Eocene (40 Ma or younger) age, respectively³⁶ (Figs. 5 and 6). Seismic horizon ASS-u1 thus forms an unconformity separating the Cretaceous (seismic unit ASS-1) from the Late Eocene strata (seismic unit ASS-2), which has a thickness of ~550 ms (~640 m using conversion velocities as derived from processing) at the location of Site PS104_21-3. The drift body down- and onlaps onto seismic horizon ASS-u2 (Fig. 2), which forms the top of seismic unit ASS-2. In this part of the ASE shelf, this reflection is observed as a conformable seismic horizon indicating non-deposition or a change in deposition. The lower part of seismic unit ASS-3 itself was sampled during RV *Polarstern* Expedition PS104 in 2017 (Site PS104_21-3 located ~12 km west of the drift, see Figs. 1, 2c and 5, cf. Klages, et al.³⁸). The dinoflagellate cysts *Lejeuneacysta katatonos* and *L. acuminata*, which have been used as regional biostratigraphic markers of the Rupelian stage in marine sediments offshore Wilkes Land and at Cape Roberts, East Antarctica^{39,40}, regularly occur at Site PS104_21-3. *Lejeuneacysta* specimen are well preserved and their dominance throughout the entire record provides no evidence of any reworking. Seismic horizon ASS-u2 can be found about 200 m below the base of Site PS104_21-3. A rough age estimate for seismic horizon ASS-u2 can be derived assuming a constant sedimentation rate for seismic units ASS-2 (~640 m thickness, max 40 Ma³⁶) and the ~200 m of sediment observed between seismic horizon ASS-u2 and the base of Site PS104_21-3 (33.8 ± 0.6 Ma³⁸). The resulting sedimentation rate of 14 cm/ky is not unrealistic³⁶. This then places seismic horizon ASS-u2 at ~35 Ma, i.e., the latest Eocene or around the Eocene/Oligocene boundary and, in combination with the biostratigraphic age, the formation of the plastered drift into the latest Eocene or earliest Oligocene.

The first advances of grounded ice to the middle shelf have been inferred for seismic units younger than ASS-3³⁵ (Fig. 6). Truncational erosion of older strata, aggradational deposition on the outer shelf and increasing formation of prograding sequences commenced in seismic unit ASS-4.

Seismic horizon ASS-u2 (Eocene/Oligocene boundary?) underlying the sediment drift (Fig. 3a) gently dips northwestward. The palaeotopographic/palaeobathymetric reconstructions of Paxman, et al.²² and Hochmuth, et al.⁴¹ for 34 Ma similarly show a seafloor rising towards the east in this area, which would have facilitated the formation of plastered drifts by low velocity bottom currents (Fig. 3b). Biostratigraphic and palaeoenvironmental evidence from sediment cores collected in the area of the West Antarctic Rift System (WARS), Marie Byrd Land⁴², provide additional constraints for the palaeo-depth of this region of West Antarctica. This is only consistent with the minimum



palaeotopography/palaeobathymetry of Paxman, et al.²² and Hochmuth, et al.⁴¹, which we therefore use for our interpretation. The minimum palaeotopography/palaeobathymetry has been adjusted for flexural isostasy (rebound for ice sheet loading) and sea level variations^{22,41}. Furthermore, the absence of an ice sheet or even the far distance to an ice sheet or high-elevation ice-cap

will not have had a significant isostatic effect on the shelf. Geometry and internal reflection configuration of a plastered drift result from the flow direction of the shaping water mass. A drift crest and the thickest accumulation document deposition to one side of the path of strongest flow, whereas erosion/non-deposition occurs below the flow path³⁴. The observed drift is plastered to

Fig. 2 Architecture of the sediment drift at the eastern flank of PIT as imaged by seismic reflection profiles. Seismic profiles AWI-20100122 (a), -20100137 (b), and -20170012 (c) show the sediment drift (the top is marked by the thick blue horizon) lying above horizon ASS-u2 (cyan). The thin blue horizons mark internal reflections of the sediment drift separating convex-up mounded subunits. Small red arrows mark reflector terminations. PS104_21-3 marks the location of the seabed drill site, where Early Oligocene sediments were recovered^{38,72}. Seismic profile AWI-20170012 further shows that the sediment drift still influences the present day seabed morphology (mounded structure above thick blue horizon). Circles with a dot in dashed ellipse mark the inferred flow direction of the deep water out of the figure plane, i.e., southwards (blue refers to flow in Early Oligocene, yellow in Pliocene/Quaternary). Seismic sections are shown in two-way travel time (TWT). The data gap in (b) results from an interruption in data acquisition due to the occurrence of marine mammals. For information on the ghost reflection see ‘Methods’. For location of seismic lines see enlarged map in Fig. 1. The uninterpreted version of the profiles can be found in Supplementary Fig. 1.

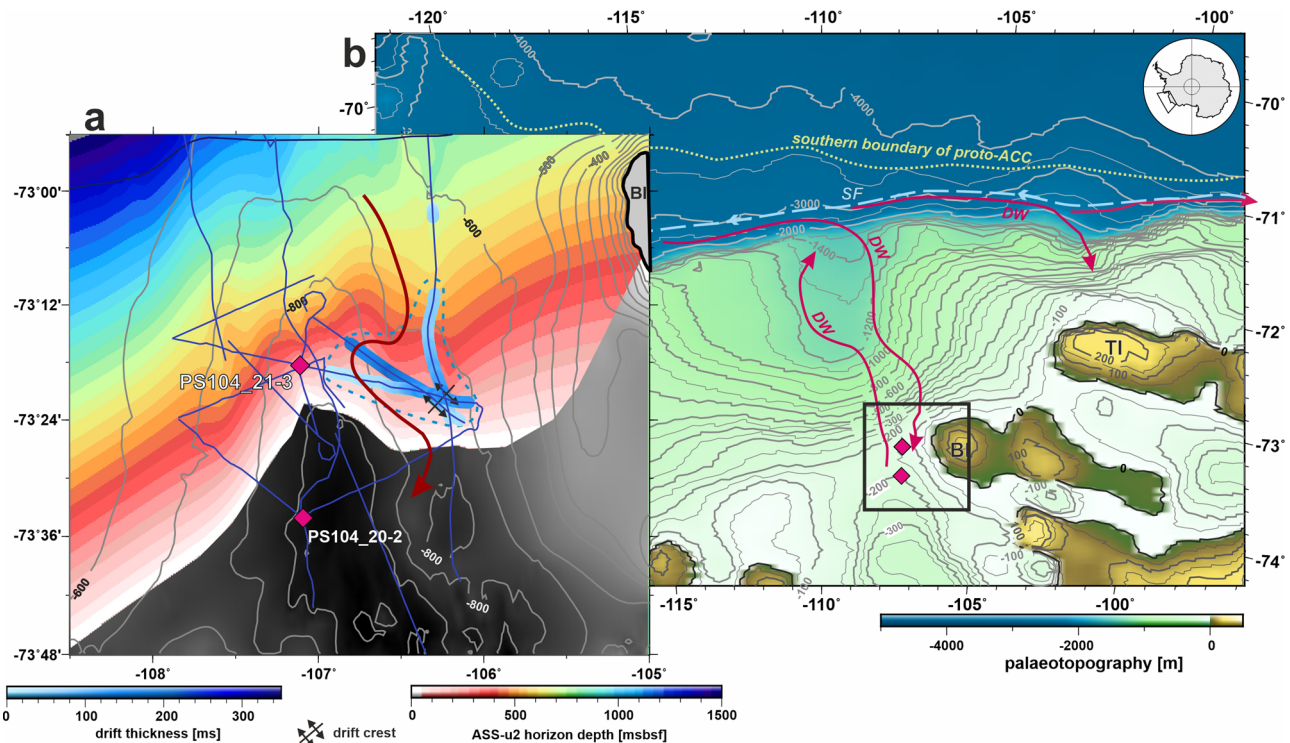


Fig. 3 Palaeobathymetry and inferred palaeocirculation. **a** Depth of seismic horizon ASS-u2 (in ms TWT below seafloor) and thickness of the imaged sediment drift lying on top of horizon ASS-u2 (in ms TWT). Dashed blue line shows inferred outline of the interpreted sediment drift. The red arrow shows the schematic deep water pathway inferred for the latest Eocene to earliest Oligocene. Thin blue lines show the location of seismic reflection profiles (for location of seismic lines shown in Figs. 2 and 5 see Fig. 1). Grey isolines and shaded area show the present day bathymetry with depths (m) labelled⁷⁸. Magenta diamonds mark locations of Sites PS104_21-3, where Early Oligocene sediments were retrieved^{38,72}, and PS104_20-2, where Late Cretaceous to Late Eocene (or younger) deposits were retrieved³⁶. BI = Burke Island. **b** Minimum palaeotopography/palaeobathymetry for the ASE^{22,41,82}. The box shows the area enlarged in (a). Magenta diamonds show the locations of Sites PS104_21-3 and PS104_20-2 in accordance with the palaeotopographic/palaeobathymetric reconstruction by Paxman, et al.²² and Hochmuth, et al.⁴¹. Arrows/lines schematically show the inferred pathways/location of deep water DW (red), potential slope front SF (dashed light blue), and the southern boundary of the proto-ACC (dashed yellow).

the eastward rising flank of seismic horizon ASS-u2 with the shallowest and thickest part in the southeast (the drift crest) (Fig. 2). The drift shows thinning towards the north and west. This drift geometry points towards a southward water mass transport (Fig. 2, open circles with dots indicate a flow path out of the figure plane, and 3, red arrow) with the Coriolis effect enhancing deposition on the left-hand side^{33,43}, i.e., the same flow direction as today’s CDW. The overall form of the sediment drift influences the present-day seabed morphology, as documented in the mounded structure observed at the seafloor on seismic profiles AWI-20170012 (CDPs 1550 to 2100) and AWI-20100137 (CDPs 600 to 1500) (Fig. 2).

Since we can rule out the formation by subglacial processes, meltwater plumes, or sediment supplied by rivers, we hypothesize that a southward flowing deep water mass, which has upwelled onto the continental shelf, shaped the observed drift between the Late Eocene and Early Oligocene. A deep water mass impinging on the shelf would have been capable of shaping the sediment

drift, as can be seen by comparison to today’s CDW^{44,45}. Deep water masses can intrude onto continental shelves due to Ekman driven pull⁴⁶ particularly where the shelf break is interrupted by troughs or canyons^{3,4} (see paleo-trough mouth/canyon in the shelf break in Figs. 3 and 7). There, they can then form shallow water sediment drifts^{47,48}. Sediments retrieved at Site PS104_20-2 about 30 km south of the observed sediment drift (Fig. 5) and at Site PS104_21-3 north of the drift northwest of the drift indicate a temperate and cool-temperate Late Eocene (Extended Data Fig. 4 of Klages, et al.)³⁶ and Early Oligocene³⁸, respectively. Material input via a coastal/estuarine system and/or resulting from biogenic productivity would have been entrained by the southward flowing deep water thus shaping the observed sediment drift (Figs. 3 and 7).

Mertz Drift on the George V Land shelf, East Antarctica, is an example for a sediment drift formed by upwelling of deep water onto the shelf and shows similarities to the drift observed on the ASE shelf. The drift is located in an ~850 m deep trough

on the shelf and covers an area of $\sim 400 \text{ km}^2$ ^{44,49}. The drift is max 20 m thick and shows a well-stratified mounded structure with a steeper flank in the southwest. It appears plastered to the eastern flank of the trough. Mertz Drift is interpreted to have been formed by modified CDW upwelling onto the shelf^{44,45,49}. Both the inflow and outflow of modified CDW entrain and transport fine-grained detritus shaping Mertz Drift. Sediment cores have shown that Mertz Drift is covered by a layer of glacimarine sediments deposited at or after the Last Glacial Maximum LGM, which, together with seismic data, indicate that Mertz Drift was formed in pre and/or at the LGM times and provides evidence for deep water upwelling onto the shelf during these times⁴⁵. The sediment drift observed on the ASE shelf has a similar spatial extent as Mertz Drift and has also been formed against a south- and westward sloping seafloor (see Fig. 3).

So far, no such sediment drifts associated with CDW have been observed in the outer parts of the western and eastern Pine Island Troughs and Abbot Trough. However, seismic coverage of the outer ASE shelf is sparse, and often a dense sea ice cover limits both the acquisition and quality of the seismic data.

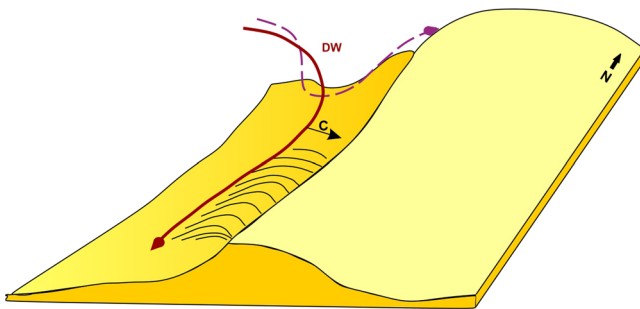


Fig. 4 Conceptual model showing formation of the sediment drift on the ASE shelf. Upwelled deep water DW (red arrow) flows southwards into the trough in the shelf break and then is steered by the eastward rising sea floor carrying/picking up sedimentary material. The DW is then deflected to the left in relation to the flow direction due to Coriolis effect (black arrow C)^{33,34}. There, the flow velocity is reduced and the material is deposited thus forming a plastered sediment drift against the sloping seafloor. With the onset of cooling, deep water is upwelled less vigorously only into the outer trough (purple dashed arrow) and then flows back into the deeper ocean.

Discussion

Observations constraining the palaeoceanography and palaeoenvironment of the Amundsen Sea during the EOT are very limited. This knowledge is essential to understand the regional and chronological development and stability of glaciation within the different sectors of Antarctica, especially in areas where today marine based ice sheets are observed¹⁷. While local ice caps at low altitudes are assumed to have existed in Marie Byrd Land as early as 29–27 Ma^{50,51}, and the WAIS may episodically have advanced onto the Ross Sea shelf during cold periods around 32 Ma already²⁰, biostratigraphic and palaeoenvironmental evidence in sediments recovered from beneath the WAIS indicate marine incursions into the WARS between the Marie Byrd Land coast and the Transantarctic Mountains for the Late Paleogene Marine Event (~ 34.5 – 31.5 Ma)⁴².

According to Paxman, et al.²², the hinterland of the ASE was mostly above sea-level at the EOT, unlike today. This suggests that any early kind of a WAIS was still far away from the shelf. Therefore, any end moraines or other glacio-morphological features documenting former ice-sheet extent would have been restricted to areas on land but not on the shelf.

Deep ocean temperatures were cooler in the Early Oligocene and the seasonality was more pronounced than during the Eocene⁵². Warmer deep water has been reported for the Wilkes Land margin and the Ross Sea^{19,53–55}. The opening of the Tasmanian Gateway has had a strong effect on the circulation and ocean temperatures near Wilkes Land^{56,57} while east of the Tasman Rise a proto-Ross gyre already existed before the opening^{56,58}. The proto-Ross gyre would have deflected oceanographic frontal systems southwards towards the continental slope at its eastern flank, where the Amundsen Sea is located, potentially driving upwelling onto the ASE shelf as observed today (Fig. 3) (e.g., refs. ^{59–61}). Therefore, the effect of the opening of the Tasmanian Gateway may not have fundamentally changed the circulation in the ASE.

Several studies suggest that conditions for a proto-Antarctic Circumpolar Current (ACC) were met already during the Late Eocene^{62–64}. This resulted in upwelling in the high-latitude South Pacific⁶³, which was further increased after opening of the Drake Passage in the Early Oligocene⁶². During warm phases in the Oligocene the westerly wind system is thought to have migrated further south, which in combination with weak easterlies and a moderate ACC flow would have favoured upwelling of deep water onto the Antarctic shelf^{19,55}, especially where troughs/canyons interrupted the shelf break^{3,4}, and therefore possibly facilitated

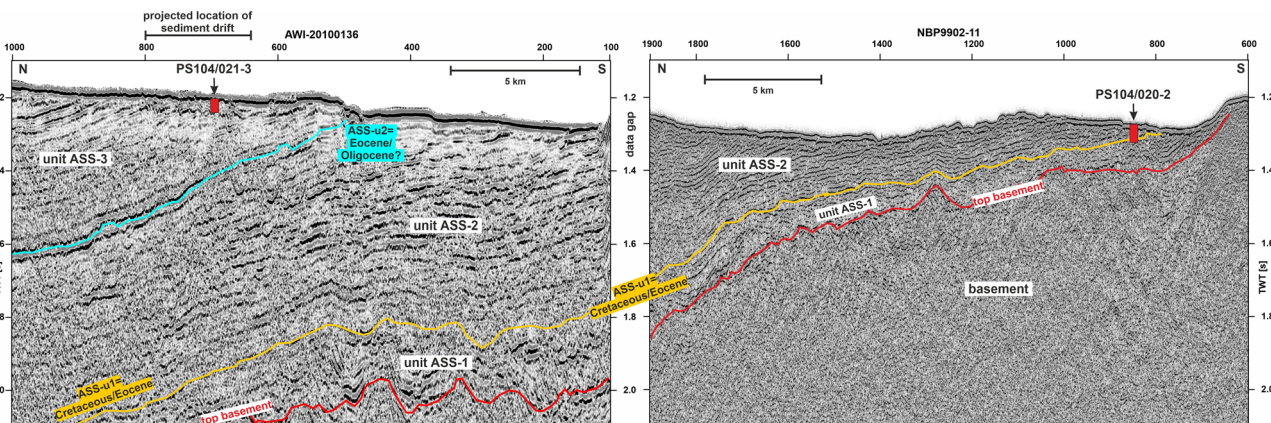


Fig. 5 Seismic transect connecting drill Sites PS104_20-2 and PS104_21-3. Note that different acquisition parameters characterise seismic profiles NBP9902-11 (single-channel)⁶⁵ and AVI-20100136 (multi-channel)³⁵ resulting in different frequency content and resolution. The red boxes show the locations and penetration of the two seabed drill sites^{36,38,72}. Seismic sections are shown in two-way travel time (TWT). For location of seismic lines see enlarged map in Fig. 1.

drift formation on the ASE shelf. A westerly wind system located further north, moderate easterlies and a weak ACC during cold phases in the Oligocene would have resulted in weak upwelling onto the shelf³⁵.

Our new seismic data have revealed a mounded structure interpreted as a sediment drift resulting from deep water upwelling onto the ASE shelf in the latest Eocene or earliest Oligocene. This upwelling was probably related to a southerly location of the ACC fronts during a warm phase. Upwelling of deep waters far onto the shelf was most likely further enhanced by the presence of a trough/channel in the ASE shelf break (Figs. 3 and 7). The deep water was then steered by the south-eastward rising seafloor and shaped the sediment drift picking up material

provided by a coastal/estuarine system or biogenic production³⁶. We propose that the intrusions of potentially warm deep water prevented a cooling of shelf waters and thus an advance of an ice sheet onto the ASE shelf during the globally observed cooling in conjunction with the EOT by buffering heat on the shelf. Later in the Oligocene, increasing global cooling will have relocated the westerly wind system northwards and influenced the intensity of

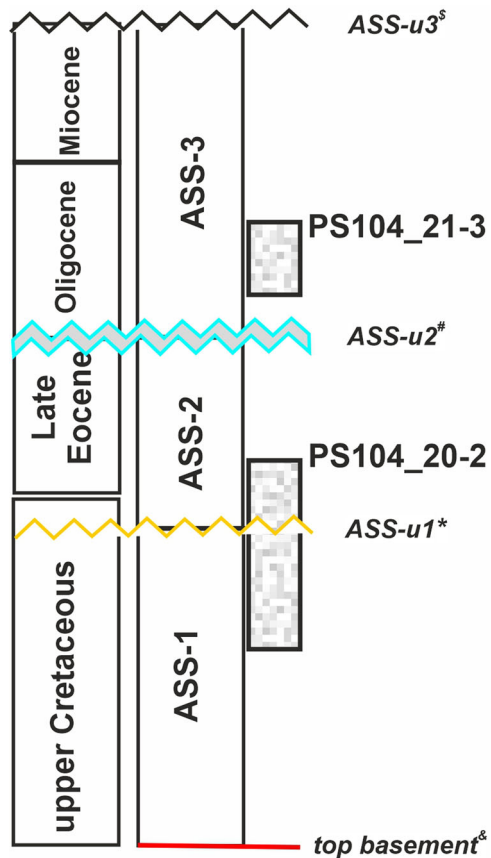


Fig. 6 Seismostratigraphic model. The model is based on the original interpretations of Gohl, et al.³⁵ (&) and Gohl, et al.³⁷ (\$) but incorporates information from Sites PS104-20-2³⁶ (*) and PS104-21-3³⁸. The age of seismic horizon ASS-u2 (#) has been inferred in this manuscript. From left to right: chronostratigraphic age, seismic units, seismic horizons, and age ranges sampled by the two seabed cores.

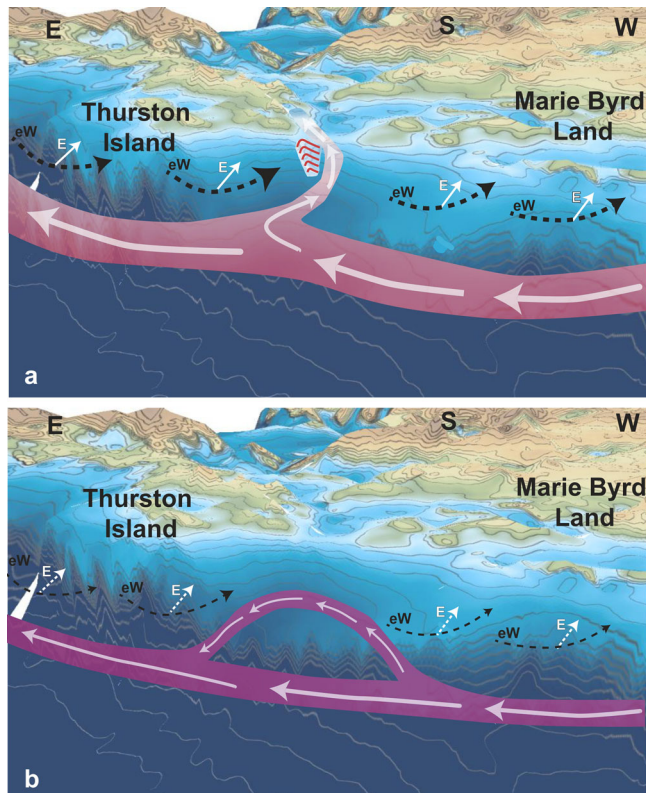


Fig. 7 Conceptual model for the upwelling of deep water onto the ASE shelf in EOT. **a** The minimum reconstruction of the palaeotopography/palaeobathymetry for 34 Ma shows a trough mouth or canyon in the shelf break^{22,41,82}, which enables the intrusion of deep water (rose arrows) onto the shelf as the result of southward Ekman transport (white E, white arrow) within the easterly winds (eW). The southward flow of deep water is steered by the higher topography on the eastern ASE shelf and shapes the sediment drift (red lines). **b** Later in the Oligocene, increasing global cooling will have relocated the wind system (eW) northwards and influenced the intensity of upwelling. Deep water (purple arrows) now can only upwell into the outer trough and is recirculated back into the deeper ocean. This may have ended the formation of the observed sediment drift plastered against seismic horizon ASS-u2 below the eastern flank of the present-day PIT. eW = easterly winds, E, S, W = East, South, West.

Table 1 Acquisition and processing parameters of used seismic data.

survey	ANT-XXVI/3	PS104	NBP9902
Seismic source	3 GI-guns	2 GI-guns	1 GI-gun
Streamer	240 channel, 3000 m active length	96 channels, 600 m active length	Single channel
Recording parameters	1 ms sample rate, 10 s record length	1 ms sample rate, 5 s record length	0.25 ms sample rate, 2 s record length
Processing parameters	25 m CDP interval, velocity analysis, nmo correction, multiple suppression fk filter, stacking, time migration	25 m CDP interval, velocity analysis, nmo correction, multiple suppression fk filter, stacking, time migration	Water column mute, bandpass filter 20–200 Hz
Display parameters	Water column mute, bandpass filter 20–200 Hz	Water column mute, bandpass filter 20–200 Hz	Water column mute, bandpass filter 20–200 Hz

upwelling. This may have ended the formation of the observed sediment drift plastered against seismic horizon ASS-u2 below the eastern flank of the present-day PIT.

The bathymetric/topographic setting in the ASE is different from the other sectors of Antarctica. Paxman, et al.²²'s minimum reconstruction for 34 Ma shows much higher elevations for East Antarctica while the Ross Sea area and the ASE are largely located below sea level. A cooling in East Antarctica thus will have had a stronger effect enabling the growth of larger ice sheets as has been suggested for the Ross Sea sector of Antarctica^{16,55}. Olivetti, et al.²⁰ also suggested Early Oligocene marine terminating ice in the Ross Sea sector but an extensive advance into the marine realm was only inferred for close to the Oligocene-Miocene boundary. The ASE shelf thus may have been the last Antarctic sector that experienced full glaciation since here oceanic circulation influenced by bathymetry appears to have delayed advance of the WAIS during the EOT. Therefore, our results highlight the importance of oceanic forcing for the evolution of the WAIS since the onset of Antarctic glaciation.

Methods

The study is based on the analysis of single- (SCS) and multichannel (MCS) seismic reflection profiles gathered in the Amundsen Sea Embayment^{65–67}. SCS line NBP9902-11 was collected using a 3.36 l GI-gun™ and a single channel streamer. The MSC data were collected with up to three GI-guns™ (1.68 l volume each GI-gun used to generate the signal) and different streamer systems (240 channel, 3000 m long in 2010, 96 channel, 600 m long streamer in 2017) (Table 1). The MCS data were recorded with a sample rate of 1 ms while line NP9902-11 was recorded with a sample rate of 0.25 ms. Standard data processing was applied to all MCS lines comprising CDP sorting, velocity analysis, stacking and migration. To suppress seafloor multiples as much as possible we applied various processing strategies including filtering in the frequency-wave number (f-k) domain prior to stacking and migration (Table 1). A ghost reflection (e.g., Fig. 2b) results from the energy traveling upward from the seismic pulse to the sea surface and there is reflected downward. This reflected ghost pulse follows the primary down going pulse by a time interval determined by the depth of the emitted seismic pulse⁶⁸. Unfortunately, processing has not always successfully suppressed the ghost reflection (see Fig. 2b). The ASE shelf is characterized by glacial overcompaction and erosion limiting the penetration of the seismic signal.

The seismic data (Supplementary Fig. 1) were analysed to identify sediment drifts, which are shaped by bottom currents. Those bottom currents comprise deep or bottom water and are driven by thermohaline circulation. They persist for long periods of time ($>10^4$ y) and can develop equilibrium conditions⁶⁹. Sediment drifts usually form asymmetric, mounded, elongated sediment bodies with a steep and a less inclined flank⁷⁰. The mounds show discontinuities at their bases and often internal discontinuities. The internal reflections show onlap and downlap onto the discontinuities as well as truncation at the top. In general, the different seismic units forming these mounds are lenticular and upward convex. The vertical stacking of the seismic units may show a lateral migration resulting from the relocation of the shaping current. Variations in climate, sea-level, and bottom circulation lead to an alternation in the dominating sediment transport process^{70,71}.

The interpretation of seismostratigraphic units and unconformities is based on Gohl, et al.³⁵ aided by age information from two shallow seabed drill cores, PS104_20-2 (for more details see Klages, et al.³⁶) and PS104_21-3 (see below, cf. Klages, et al.³⁸). The seismostratigraphic analysis of a set of seismic reflection data from the ASE shelf and slope revealed six major sedimentary units (ASS-1 to ASS-6, ASS = Amundsen Sea Shelf) separated by five major erosional unconformities (ASS-u1 to ASS-u5) from bottom to top. Via a comparison of the observed seismic characteristics with those of other Antarctic shelf sequences ages were assigned to the different sedimentary units. With the aid of the two shallow seabed drill cores taken in 2017⁷², seismic horizon ASS-u1 was dated to represent a hiatus from the Late Cretaceous to at least the Late Eocene³⁶, unit ASS-2 was interpreted as Late Eocene-Oligocene (?)³⁶ and unit ASS-3 was assigned to the Oligocene to Miocene.

Core PS104_21-3 was collected during RV *Polarstern* expedition PS104 in 2017 using a remotely operated seafloor drill rig. For technical and operational details see Gohl, et al.⁷². We reconstructed the position of the drill sites in Fig. 3 in accordance with the palaeotopographic/palaeobathymetric reconstruction by Paxman, et al.²² and Hochmuth, et al.⁴¹.

A total of seven samples from core PS104_21-3 have been processed for biostratigraphic (palynological) analyses following standard palynological techniques, including sieving (10 µm) and acid treatment with 10% HCl (Hydrochloric acid) and cold 38% HF (Hydrofluoric acid). The samples showed a general low diversity of dinoflagellate cysts with a dominance of taxa of the genus *Lejeuneacysta*, including the age indicative *L. katatonos* and *L. acuminata*.

Data availability

All data needed to evaluate the conclusions in the paper are present in the main text or the Supplementary materials. All data are publicly available at the following repositories: AWI seismic data, Pangaea (<https://doi.org/10.1594/PANGAEA.933264>, <https://doi.org/10.1594/PANGAEA.933266>, <https://doi.org/10.1594/PANGAEA.933265>^{73–76}, NBP9902 seismic data, IEDA (<https://doi.org/10.1594/IEDA/307363>)⁷⁷.

Received: 29 June 2021; Accepted: 31 January 2022;

Published online: 21 February 2022

References

- Drewry, D. J., Jordan, S. R. & Jankowski, E. Measured properties of the antarctic ice sheet: surface configuration, ice thickness, volume and bedrock characteristics. *Ann. Glaciol.* **3**, 83–91 (1982).
- Rignot, E. et al. Four decades of Antarctic ice sheet mass balance from 1979–2017. *Proc. Natl Acad. Sci. USA* **116**, 1095–1103 (2019).
- Assmann, K. M. et al. Variability of circumpolar deep water transport onto the amundsen sea continental shelf through a shelf break trough. *J. Geophys. Res.: Oceans* **118**, 6603–6620 (2013).
- Walker, D. P., Jenkins, A., Assmann, K. M., Shoosmith, D. R. & Brandon, M. A. Oceanographic observations at the shelf break of the Amundsen Sea, Antarctica. *J. Geophys. Res.: Oceans* **118**, 2906–2918 (2013).
- Jacobs, S. S., Hellmer, H. H. & Jenkins, A. Antarctic Ice Sheet melting in the southeast Pacific. *Geophys. Res. Lett.* **23**, 957–960 (1996).
- Jacobs, S. S., Jenkins, A., Giulivi, C. F. & Dutrieux, P. Stronger ocean circulation and increased melting under Pine Island Glacier ice shelf. *Nature Geosci.* **4**, 519–523 (2011).
- Jenkins, A. et al. West Antarctic Ice Sheet retreat in the Amundsen Sea driven by decadal oceanic variability. *Nature Geosci.* **11**, 733–738 (2018).
- Joughin, I. & Alley, R. B. Stability of the West Antarctic ice sheet in a warming world. *Nature Geosci.* **4**, 506–513 (2011).
- Hillenbrand, C.-D. et al. West Antarctic Ice Sheet retreat driven by Holocene warm water incursions. *Nature* **547**, 43–48 (2017).
- Pollard, D. & DeConto, R. M. Modelling West Antarctic ice sheet growth and collapse through the past five million years. *Nature* **458**, 329–332 (2009).
- Sutter, J. et al. Modelling the Antarctic Ice Sheet across the mid-Pleistocene transition—implications for Oldest Ice. *Cryosphere* **13**, 2023–2041 (2019).
- Lear, C. H., Bailey, T. R., Pearson, P. N., Coxall, H. K. & Rosenthal, Y. Cooling and ice growth across the Eocene-Oligocene transition. *Geology* **36**, 251–254 (2008).
- Westerhold, T. et al. An astronomically dated record of Earth's climate and its predictability over the last 66 million years. *Science* **369**, 1383–1387 (2020).
- Hutchinson, D. K. et al. The Eocene–Oligocene transition: a review of marine and terrestrial proxy data, models and model–data comparisons. *Clim. Past* **17**, 269–315 (2021).
- Passchier, S., Ciarletta, D. J., Miragos, T. E., Bijl, P. K. & Bohaty, S. M. An Antarctic stratigraphic record of stepwise ice growth through the Eocene–Oligocene transition. *Geol. Soc. Am. Bull.* **129**, 318–330 (2017).
- Galeotti, S. et al. Antarctic Ice Sheet variability across the Eocene–Oligocene boundary climate transition. *Science* **352**, 76–80 (2016).
- O'Brien, C. L. et al. The enigma of Oligocene climate and global surface temperature evolution. *Proc. Natl Acad. Sci. USA* **117**, 25302–25309 (2020).
- Palike, H. et al. The heartbeat of the oligocene climate system. *Science* **314**, 1894–1898 (2006).
- Bijl, P. K. et al. Paleoceanography and ice sheet variability offshore Wilkes Land, Antarctica—Part 2: Insights from Oligocene–Miocene dinoflagellate cyst assemblages. *Clim. Past* **14**, 1015–1033 (2018).
- Olivetti, V. et al. Evidence of a full West Antarctic Ice Sheet back to the early Oligocene: insight from double dating of detrital apatites in Ross Sea sediments. *Terra Nova* **27**, 238–246 (2015).
- Hochmuth, K. & Gohl, K. Seaward growth of Antarctic continental shelves since establishment of a continent-wide ice sheet: Patterns and mechanisms. *Palaeogeogr. Palaeoclimatol. Palaeoecol.* **520**, 44–54 (2019).
- Paxman, G. J. G. et al. Reconstructions of Antarctic topography since the Eocene–Oligocene boundary. *Palaeogeogr. Palaeoclimatol. Palaeoecol.* **535**, 109346 (2019).
- Kennedy-Asser, A. T. et al. Changes in the high-latitude Southern Hemisphere through the Eocene–Oligocene transition: a model–data comparison. *Clim. Past* **16**, 555–573 (2020).
- Batchelor, C. L. & Dowdeswell, J. A. Ice-sheet grounding-zone wedges (GZWs) on high-latitude continental margins. *Marine Geol.* **363**, 65–92 (2015).
- Batchelor, C. L., Dowdeswell, J. A. & Ottesen, D. In *Submarine Geomorphology* (eds Aaron Micallef, Sebastian Krastel, & Alessandra Savini) 207–234 (Springer International Publishing, 2018).

26. Faugères, J. C. & Stow, D. A. V. In *Developments in Sedimentology* Vol. 60 (eds. M. Rebasco & A. Camerlenghi) 257, 259–288 (Elsevier, 2008).
27. Knutz, P. C., Hopper, J. R., Gregersen, U., Nielsen, T. & Japsen, P. A contourite drift system on the Baffin Bay–West Greenland margin linking Pliocene Arctic warming to poleward ocean circulation. *Geology* **43**, 907–910 (2015).
28. Rebasco, M., Hernández-Molina, F. J., Van Rooij, D. & Wählén, A. Contourites and associated sediments controlled by deep-water circulation processes: State-of-the-art and future considerations. *Marine Geol.* **352**, 111–154 (2014).
29. Faugères, J. C., Stow, D. A. V., Imbert, P. & Viana, A. R. Seismic features diagnostic of contourite drifts. *Marine Geol.* **162**, 1–38 (1999).
30. Preu, B. et al. Morphosedimentary and hydrographic features of the northern Argentine margin: The interplay between erosive, depositional and gravitational processes and its conceptual implications. *Deep Sea Res. Part I: Oceanogr. Res. Pap.* **75**, 157–174 (2013).
31. Grützner, J., Uenzelmann-Neben, G. & Franke, D. Variations in bottom water activity at the southern Argentine margin: indications from a seismic analysis of a continental slope terrace. *Geo Marine Lett.* **31**, 405–417 (2011).
32. Grützner, J., Uenzelmann-Neben, G. & Franke, D. Variations in sediment transport at the central Argentine continental margin during the Cenozoic. *Geochem. Geophys. Geosyst.* **13**, Q10003 (2012).
33. Cossu, R. & Wells, M. G. The evolution of submarine channels under the influence of Coriolis forces: experimental observations of flow structures. *Terra Nova* **25**, 65–71 (2013).
34. Cossu, R., Wells, M. G. & Wählén, A. K. Influence of the Coriolis force on the velocity structure of gravity currents in straight submarine channel systems. *J. Geophys. Res.* **115**, C11016 (2010).
35. Gohl, K. et al. Seismic stratigraphic record of the Amundsen Sea Embayment shelf from pre-glacial to recent times: Evidence for a dynamic West Antarctic ice sheet. *Marine Geol.* **344**, 115–131 (2013).
36. Klages, J. P. et al. Temperate rainforests near the South Pole during peak Cretaceous warmth. *Nature* **580**, 81–86 (2020).
37. Gohl, K. et al. Evidence for a Highly Dynamic West Antarctic Ice Sheet During the Pliocene. *Geophys. Res. Lett.* **48**, e2021GL093103 (2021).
38. Klages, J. et al. West Antarctic archipelago covered by cool-temperate forests during early Oligocene glaciation. in *EGU General Assembly 2021*, <https://doi.org/10.5194/egusphere-egu21-1538> (online, 2021).
39. Bijl, P. K., Houben, A. J. P., Bruls, A., Pross, J. & Sangiorgi, F. Stratigraphic calibration of Oligocene–Miocene organic-walled dinoflagellate cysts from offshore Wilkes Land, East Antarctica, and a zonation proposal. *J. Micropalaeontol.* **37**, 105–138 (2018).
40. Clowes, C. D., Hannah, M. J., Wilson, G. J. & Wrenn, J. H. Marine palynostratigraphy and new species from the Cape Roberts drill-holes, Victoria land basin, Antarctica. *Marine Micropaleontology* **126**, 65–84 (2016).
41. Hochmuth, K. et al. Combined palaeotopography and palaeobathymetry of the Antarctic continent and the Southern Ocean since 34 Ma. <https://doi.org/10.1594/PANGAEA.918663> (PANGAEA, 2020).
42. Coenen, J. J. et al. Paleogene Marine and Terrestrial Development of the West Antarctic Rift System. *Geophys. Res. Lett.* **47**, e2019GL085281 (2020).
43. Cossu, R. & Wells, M. G. Coriolis forces influence the secondary circulation of gravity currents flowing in large-scale sinuous submarine channel systems. *Geophys. Res. Lett.* **37**, <https://doi.org/10.1029/2010GL044296> (2010).
44. Presti, M., De Santis, L., Brancolini, G. & Harris, P. T. Continental shelf record of the East Antarctic Ice Sheet evolution: seismo-stratigraphic evidence from the George V Basin. *Quaternary Sci. Rev.* **24**, 1223–1241 (2005).
45. Presti, M., De Santis, L., Busetti, M. & Harris, P. T. Late Pleistocene and Holocene sedimentation on the George V Continental Shelf, East Antarctica. *Deep Sea Res. Part II: Top. Stud. Oceanogr.* **50**, 1441–1461 (2003).
46. Rintoul, S. R., Hughes, C. W. & Olbers, D. In *Ocean Circulation and Climate* Vol. 77 (eds. G. Siedler, J. A. Church, & J. Gould) Ch. 4.6, 271–302 (Academic Press, 2001).
47. Séranne, M. & Nzé Abeigne, C.-R. Oligocene to Holocene sediment drifts and bottom currents on the slope of Gabon continental margin (west Africa): Consequences for sedimentation and southeast Atlantic upwelling. *Sediment. Geol.* **128**, 179–199 (1999).
48. Yoon, S. H. & Chough, S. K. Sedimentary characteristics of Late Pleistocene bottom-current deposits, Barents Sea slope off northern Norway. *Sediment. Geol.* **82**, 33–45 (1993).
49. Verdicchio, G. & Trincardi, F. In *Developments in Sedimentology* Vol. Volume 60 (eds. M. Rebasco & A. Camerlenghi) 409–433 (Elsevier, 2008).
50. Rocchi, S., LeMasurier, W. E. & Di Vincenzo, G. Oligocene to Holocene erosion and glacial history in Marie Byrd Land, West Antarctica, inferred from exhumation of the Dorrel Rock intrusive complex and from volcano morphologies. *Geol. Soc. Am. Bull.* **118**, 991–1005 (2006).
51. Wilch, T. I. & McIntosh, W. C. Eocene and Oligocene volcanism at Mount Petras, Marie Byrd Land: implications for middle Cenozoic ice sheet reconstructions in West Antarctica. *Antarct. Sci.* **12**, 477–491 (2000).
52. Huber, M. & Nof, D. The ocean circulation in the southern hemisphere and its climatic impacts in the Eocene. *Palaeogeogr. Palaeoclimatol. Palaeoecol.* **231**, 9–28 (2006).
53. Evangelinos, D. et al. Late oligocene-miocene proto-antarctic circumpolar current dynamics off the Wilkes Land margin, East Antarctica. *Glob. Planet. Change* **191**, 103221 (2020).
54. Salabarnada, A. et al. Paleoceanography and ice sheet variability offshore Wilkes Land, Antarctica—Part 1: Insights from late Oligocene astronomically paced contourite sedimentation. *Clim. Past* **14**, 991–1014 (2018).
55. Levy, R. H. et al. Antarctic ice-sheet sensitivity to obliquity forcing enhanced through ocean connections. *Nat. Geosci.* **12**, 132–137 (2019).
56. Stickley, C. E. et al. Timing and nature of the deepening of the Tasmanian Gateway. *Paleoceanography* **19**, PA4027 (2004).
57. Bijl, P. K. et al. Eocene cooling linked to early flow across the Tasmanian Gateway. *Proc. Natl Acad. Sci. USA* **110**, 9645–9650 (2013).
58. Huber, M. et al. Eocene circulation of the Southern Ocean: Was Antarctica kept warm by subtropical waters? *Paleoceanography* **19**, PA4026 (2004).
59. Thoma, M., Jenkins, A., Holland, D. M. & Jacobs, S. Modelling circumpolar deep water intrusions on the Amundsen Sea continental shelf, Antarctica. *Geophys. Res. Lett.* **35**, L18602 (2008).
60. Orsi, A. H., Whitworth, T. & Nowlin, W. D. On the meridional extent and fronts of the Antarctic Circumpolar Current. *Deep Sea Res. Part I: Oceanogr. Res. Pap.* **42**, 641–673 (1995).
61. Jacobs, S. et al. The Amundsen Sea and the Antarctic Ice Sheet. *Oceanogr.* **25**, <https://doi.org/10.5670/oceanog.2012.90> (2012).
62. Scher, H. D. & Martin, E. E. Oligocene deep water export from the North Atlantic and the development of the Antarctic Circumpolar Current examined with neodymium isotopes. *Paleoceanography* **23**, PA1205 (2008).
63. Sarkar, S. et al. Late Eocene onset of the proto-Antarctic circumpolar current. *Sci. Rep.* **9**, 10125 (2019).
64. Scher, H. D. & Martin, E. E. Timing and climatic consequences of the opening of Drake Passage. *Science* **312**, 428–430 (2006).
65. Lowe, A. J. & Anderson, J. B. Reconstruction of the West Antarctic ice sheet in Pine Island Bay during the Last Glacial Maximum and its subsequent retreat history. *Quaternary Sci. Rev.* **21**, 1879–1897 (2002).
66. Gohl, K. The expedition of the Research Vessel “Polarstern”; ANT-XXVI/3 29 January–5 April 2010 Wellington Punta Arenas 173 (Alfred-Wegener-Institut, Bremerhaven, 2010).
67. Gohl, K. The Expedition PS104 of the Research Vessel POLARSTERN to the Amundsen Sea in 2017. 100 (Alfred Wegener Institute for Polar and Marine Research, Bremerhaven, 2017).
68. Yilmaz, Ö. *Seismic Data Analysis*. Vol. 10 (Society of Exploration Geophysicists, 2001).
69. Zenk, W. In *Developments in Sedimentology* Vol. 60, 37–57 (Elsevier, 2008).
70. Stow, D. A. V., Faugères, J.-C., Howe, J. A., Pudsey, C. J. & Viana, A. R. In *Deep-water contourite systems: Modern drifts and ancient series* Vol. 22 *Memoir* (eds. D. A. V. Stow et al.) 7–20 (Geological Society of London, 2002).
71. Faugères, J. C., Mezerais, M. L. & Stow, D. A. V. Bottom-controlled sedimentation: a synthesis of the contourite problem. *Sediment. Geol.* **82**, 287–297 (1993).
72. Gohl, K. et al. MeBo70 Seabed drilling on a polar continental shelf: operational report and lessons from drilling in the amundsen sea embayment of West Antarctica. *Geochem. Geophys. Geosyst.* **18**, 4235–4250 (2017).
73. Uenzelmann-Neben, G. & Gohl, K. Amundsen Sea Shelf, seismic reflection profile AWI-20100122 (PANGAEA, 2021). <https://doi.pangaea.de/10.1594/PANGAEA.933264>.
74. Uenzelmann-Neben, G. & Gohl, K. Amundsen Sea Shelf, seismic reflection profile AWI-20100136 (PANGAEA, 2021). <https://doi.pangaea.de/10.1594/PANGAEA.933266>.
75. Uenzelmann-Neben, G. & Gohl, K. Amundsen Sea Shelf, seismic reflection profile AWI-20100137 (PANGAEA, 2021). <https://doi.pangaea.de/10.1594/PANGAEA.933265>.
76. Uenzelmann-Neben, G. & Gohl, K. Amundsen Sea Shelf, seismic reflection profile AWI-20170012 (PANGAEA, 2021). <https://doi.pangaea.de/10.1594/PANGAEA.933269>.
77. Anderson, J. In *Interdisciplinary Earth Data Alliance (IEDA)* (2007).
78. Arndt, J. E. et al. The International Bathymetric Chart of the Southern Ocean (IBCSO) Version 1.0—A new bathymetric compilation covering circum-Antarctic waters. *Geophys. Res. Lett.* **40**, 3111–3117 (2013).
79. Orsi, A. H., Johnson, G. C. & Bullister, J. L. Circulation, mixing, and production of Antarctic Bottom Water. *Prog. Oceanogr.* **43**, 55–109 (1999).
80. Nakayama, Y., Schröder, M. & Hellmer, H. H. From circumpolar deep water to the glacial meltwater plume on the eastern Amundsen Shelf. *Deep Sea Res. Part I: Oceanogr. Res. Pap.* **77**, 50–62 (2013).
81. Thompson, A. F., Speer, K. G. & Schulze Chretien, L. M. Genesis of the Antarctic slope current in West Antarctica. *Geophys. Res. Lett.* **47**, e2020GL087802 (2020).

82. Hochmuth, K. et al. The evolving paleobathymetry of the circum-antarctic southern ocean since 34 Ma: a key to understanding past cryosphere-ocean developments. *Geochem. Geophys. Geosyst.* **21**, e2020GC009122 (2020).

Acknowledgements

We thank the captains and crews of RV *Polarstern* Expeditions ANT-XXVI/3 and PS104, as well as the MARUM-MeBo70 and the seismic teams for their support. We further thank Brian Romans and two anonymous reviewers for their very helpful comments and suggestions, which improved the manuscript. The authors would like to thank Emerson E&P Software, Emerson Automation Solutions, for providing licenses for their seismic processing and mapping software Paradigm in the scope of the Emerson Academic Program. The operation of the MARUM-MeBo70 Sea Floor Drill Rig was funded by the Alfred Wegener Institute (AWI) through its Research Program PACES II Topic 3 and grant no. AWI_PS104_001, the MARUM Center for Marine Environmental Sciences, the British Antarctic Survey through its Polar Science for Planet Earth programme, and the Natural Environmental Research Council funded UK IODP programme. G.U.-N., K.G. and J.P.K. were funded by the AWI PACES II programme. J.P.K. was further funded by the Helmholtz Association (PD-201). BAS and NERC UK IODP funded UK participation in expedition PS104.

Author contributions

G.U.-N. conceived the idea and led the study, and together with K.G., K.H., U.S. and R.D.L. wrote the manuscript with contributions from all co-authors. J.P.K. and C.-D.H. led the analytical program of the MeBo drill cores, and U.S. provided the biostratigraphic age. G.U.-N., K.G., K.H. and R.D.L. undertook the seismic surveys, and G.U.-N. and K.G. processed the seismic data. All members of the Expedition PS104 Science Team helped in pre-site survey investigations, core recovery, on-board analyses and/or shore based measurements. K.G., G.U.-N., R.D.L. and C.-D.H. acquired funding, and amongst others, proposed, and planned RV *Polarstern* expeditions ANT-XXVI/3 and PS104. All co-authors commented on the manuscript and provided input to its final version.

Funding

Open Access funding enabled and organized by Projekt DEAL.

Science Team of Expedition PS104

V. Afanasyeva⁵, J. E. Arndt¹, T. Bickert⁶, S. M. Bohaty⁷, R. Dziadek¹, B. Ebermann⁸, W. Ehrmann⁹, O. Esper¹, T. Frederichs¹⁰, T. Freudenthal⁶, C. Gebhardt¹, K. Küssner¹, G. Kuhn¹, Y. Najman¹¹, H. Pälike⁶, F. Rieftahl¹, T. Ronge¹, M. Scheinert⁸, P. Simoes Pereira¹², J. A. Smith⁴, C. Spiegel¹⁰, T. Van de Flierdt¹² & M. Zundel¹⁰

⁵VNIIOkeangeologie, St Petersburg, Russia. ⁶MARUM—Center for Marine Environmental Sciences, Bremen, Germany. ⁷University of Southampton, Southampton, UK. ⁸Technische Universität Dresden, Dresden, Germany. ⁹University of Leipzig, Institute for Geophysics and Geology, Leipzig, Germany. ¹⁰University of Bremen, Faculty of Geosciences, Bremen, Germany. ¹¹Lancaster Environment Centre, Lancaster University, Lancaster, UK. ¹²Imperial College London, Department of Earth Science & Engineering, London, UK.

Competing interests

The authors declare no competing interests.

Additional information

Supplementary information The online version contains supplementary material available at <https://doi.org/10.1038/s43247-022-00369-x>.

Correspondence and requests for materials should be addressed to Gabriele Uenzelmann-Neben.

Peer review information *Communications Earth & Environment* thanks Brian Romans, Tanghua Li and the other, anonymous, reviewer(s) for their contribution to the peer review of this work. Primary Handling Editors: Adam Switzer, Joe Aslin.

Reprints and permission information is available at <http://www.nature.com/reprints>

Publisher's note Springer Nature remains neutral with regard to jurisdictional claims in published maps and institutional affiliations.



Open Access This article is licensed under a Creative Commons Attribution 4.0 International License, which permits use, sharing, adaptation, distribution and reproduction in any medium or format, as long as you give appropriate credit to the original author(s) and the source, provide a link to the Creative Commons license, and indicate if changes were made. The images or other third party material in this article are included in the article's Creative Commons license, unless indicated otherwise in a credit line to the material. If material is not included in the article's Creative Commons license and your intended use is not permitted by statutory regulation or exceeds the permitted use, you will need to obtain permission directly from the copyright holder. To view a copy of this license, visit <http://creativecommons.org/licenses/by/4.0/>.

© The Author(s) 2022